J Sci Comput (2015) 62:555–574
DOI 10.1007/s10915-014-9869-2

Asymptotic-Preserving Exponential Methods for the Quantum Boltzmann Equation with High-Order Accuracy

Jingwei Hu · Qin Li · Lorenzo Pareschi

Received: 23 October 2013 / Revised: 3 May 2014 / Accepted: 8 May 2014 /
Published online: 16 May 2014

Abstract In this paper we develop high order asymptotic preserving methods for the spatially inhomogeneous quantum Boltzmann equation. We follow the work in Li and Pareschi (J Comput Phys 259:402–420, 2014) where asymptotic preserving exponential Runge–Kutta methods for the classical inhomogeneous Boltzmann equation were constructed. A major difficulty here is related to the non Gaussian steady states characterizing the quantum kinetic behavior. We show that the proposed schemes achieve high-order accuracy uniformly in time for all Planck constants ranging from classical regime to quantum regime, and all Knudsen number ranging from kinetic regime to fluid regime. Computational results are presented for both Bose gas and Fermi gas.

Keywords Quantum Boltzmann equation · Asymptotic preserving methods · Exponential Runge–Kutta schemes

Mathematics Subject Classification 65L04 · 65L06 · 35Q20 · 82C10

This work was partially supported by RNMS11-07444 (KI-Net) and by PRIN 2009 project "Advanced numerical methods for kinetic equations and balance laws with source terms".

J. Hu
Institute for Computational Engineering and Sciences (ICES) and Bureau of Economic Geology (BEG), The University of Texas at Austin, 201 East 24th St, Stop C0200, Austin, TX 78712, USA
e-mail: hu@ices.utexas.edu

Q. Li (✉)
Department of Computing + Mathematical Sciences (CMS), The Annenberg Center, California Institute of Technology, 1200 E. California Blvd., Pasadena, CA 91125, USA
e-mail: qinli@caltech.edu

L. Pareschi
Department of Mathematics and Computer Science, University of Ferrara, Via Machiavelli 35, 44121 Ferrara, Italy
e-mail: lorenzo.pareschi@unife.it

1 Introduction

The quantum Boltzmann equation (QBE), also known as the Nordheim-Uehling-Uhlenbeck equation, describes the non-equilibrium dynamics of a dilute quantum gas consisting of elementary particles of bosons or fermions [3]. With the quantum information embedded in the collision term, this equation gives better description to quantum particles, and it recovers the standard Boltzmann equation for the classical particles in the zero limit of the Planck constant, and thus covers a wider range of particle behavior. The QBE and its variants have many applications in science and engineering, including the kinetic description of Bose–Einstein condensate [31,33], and the modeling of electron interactions in semiconductor devices [18,24].

In this paper we design a class of high order numerical methods for quantum Boltzmann equation, that is accurate and efficient in both kinetic and hydrodynamic regimes for all Planck constants. In kinetic theory, the time discretization represents a computational challenge in the construction of numerical methods, especially in stiff regimes, when the collisional scale becomes dominant over the transport of particles, and the fluid-dynamic limit is achieved. To resolve the collision term, the time step is severely controlled by the Knudsen number for numerical stability if explicit schemes are used. On the other hand, though the implicit schemes allows larger time steps for stability, they are impractical due to the nonlinear and nonlocal collision operator.

Many techniques have been developed to address such issues in recent years, and we specifically mention the micro-macro decomposition [2], the BGK penalization method [9], and the exponential Runge–Kutta methods [6,10]. The feature shared among these techniques is that the schemes are unconditionally stable, capturing the asymptotic limits automatically with time step relaxed from the constraints of the Knudsen number, and therefore, numerically less complicated than other possible approaches, for example, the domain decomposition strategies and hybrid methods at different levels [4,5,27,34]. For a nice survey on asymptotic-preserving (AP) scheme for various kinds of systems see, for instance, the review paper by Jin [17]. In the case of Boltzmann-type kinetic equations we refer to a recent review by Pareschi and Russo [29].

In this work we extend the asymptotic preserving exponential Runge–Kutta method developed in [6,20] to the quantum Boltzmann equation. The extension to the multi-species Boltzmann equation was done in [21]. We refer the reader to [13] for an introduction to time integration exponential techniques. The discussion on AP property and stability can be found in [6,28]. New difficulties in the quantum case would be:

- The steady states are not classical Maxwellian (Gaussian distribution) and to obtain the local equilibrium—the quantum Maxwellian (Bose–Einstein or Fermi–Dirac distribution), a nonlinear system needs to be inverted;
- The methods developed need to be uniformly high order and efficient for all Planck constants, and capture the classical limit.

An asymptotic-preserving method for the quantum Boltzmann equation has been proposed in [8], where a first-order IMEX scheme combined with the standard BGK penalization idea was used. In particular, the classical Maxwellian was suggested in [8] as an alternative to the complicated quantum Maxwellian for penalty. This replacement saves fairly amount of computational cost, but the price to pay is the loss of the strong AP property (namely, in the fluid-limit the distribution function should converge in one time step to its physical equilibrium state). Moreover, as the scheme is of IMEX type, it is hard to extend the method to very high order [7]. In comparison, our new schemes possess the strong AP property and, in

principle, could achieve arbitrarily high order. As we shall see, the presence of non classical steady states has a profound influence on the structure of the resulting numerical method.

Let us finally recall that the construction of numerical methods for the full problem involves also discretization of the space and velocity variables. The latter discretization in particular is a challenging problem for the Boltzmann equation due to the high-dimensionality of the collision operator [8,11,16,25] and the occurrence of the Bose–Einstein condensation phenomenon in the degenerate quantum case [22,23]. Here, however, we do not discuss further these issues.

The rest of the paper is organized as follows. In Sect. 2 we review some basic features of the quantum Boltzmann equation and its Euler limit. We emphasize in particular the differences between the classical and the quantum equilibrium states. Next in Sect. 3 we introduce the general form of the asymptotic-preserving exponential methods for the quantum Boltzmann equation. The properties of the method are then analyzed in Sect. 4. Several numerical examples are reported in Sect. 5 to show the AP property and the high-order accuracy of the schemes. We conclude the paper with some remarks in the last section.

2 The Quantum Boltzmann Equation and Its Euler Limit

The quantum Boltzmann equation was first formulated by Nordheim, Uehling and Uhlenbeck from the classical Boltzmann equation through heuristic arguments [26,35]. In its dimensionless form, the equation writes as:

$$\partial_t f + v \cdot \nabla_x f = \frac{1}{\varepsilon} Q_q(f), \qquad t \geq 0, \quad x \in \Omega \subset \mathbb{R}^d, \quad v \in \mathbb{R}^d, \quad d = 2, 3, \tag{2.1}$$

where $f(t, x, v)$ is the phase space distribution function representing the (rescaled) number of particles that travel with velocity v at location x and time t. ε is the so-called Knudsen number defined as the ratio of the mean free path over the typical length scale. It could vary across scales from $\varepsilon \sim \mathcal{O}(1)$ to $\varepsilon \ll 1$, depending on which, the system falls into the kinetic regime or fluid regime, respectively. The collision operator Q_q models the interaction between quantum particles (here and in the rest of the paper, we always use the upper sign to denote the Bose gas and the lower sign to the Fermi gas):

$$Q_q(f) = \int_{\mathbb{R}^d} \int_{\mathbb{S}^{d-1}} B(v - v_*, \sigma)[f' f'_*(1 \pm \theta_0 f)(1 \pm \theta_0 f_*) - f f_*(1 \pm \theta_0 f')(1 \pm \theta_0 f'_*)] \mathrm{d}\sigma \mathrm{d}v_*, \tag{2.2}$$

where as usual, f, f_*, f', and f'_* are short notations for $f(t, x, v)$, $f(t, x, v_*)$, $f(t, x, v')$, and $f(t, x, v'_*)$. (v, v_*) and (v', v'_*) are the velocities before and after collision:

$$\begin{cases} v' = \frac{v+v_*}{2} + \frac{|v-v_*|}{2}\sigma, \\ v'_* = \frac{v+v_*}{2} - \frac{|v-v_*|}{2}\sigma, \end{cases} \tag{2.3}$$

where σ is the unit vector along $v' - v'_*$. Then the operator (2.2) can formally be split, in a self-evident way, into a gain and a loss term,

$$Q_q(f) = Q_q^+(f) - f Q_q^-(f). \tag{2.4}$$

The collision kernel B is a nonnegative function that only depends on $|v - v_*|$ and $\cos\theta$ (θ is the angle between σ and $v - v_*$). For variable hard sphere (VHS) particles, B is independent of scattering angle:

$$B = C_\gamma |v - v_*|^\gamma, \tag{2.5}$$

where $\gamma = 0$ corresponds to the Maxwell molecules, and $\gamma = 1$ is the hard sphere model. The parameter θ_0 is some constant proportional to the Planck constant:[1]

$$\theta_0 = C\hbar^d. \tag{2.6}$$

It characterizes the degree of degeneracy of the system in the sense that when $\theta_0 \to 0$, one recovers the collision operator for classical particles:

$$\mathcal{Q}_c(f) = \int_{\mathbb{R}^d} \int_{\mathbb{S}^{d-1}} B(v - v_*, \sigma)[f' f'_* - f f_*] \mathrm{d}\sigma \, \mathrm{d}v_*. \tag{2.7}$$

Compared with $\mathcal{Q}_c$, the quantum Boltzmann operator $\mathcal{Q}_q$ involves more nonlinearity (it is cubic rather than quadratic). This new feature brings more complexities to both theoretical and numerical studies. We are particularly interested in the fluid regime, where macroscopic equations can be derived similarly as the classical case. To this aim, we first summarize the basic properties of $\mathcal{Q}_q$.

1. $\mathcal{Q}_q$ conserves mass, momentum, and energy:

$$\int_{\mathbb{R}^d} \mathcal{Q}_q(f) \, \mathrm{d}v = \int_{\mathbb{R}^d} \mathcal{Q}_q(f) v \, \mathrm{d}v = \int_{\mathbb{R}^d} \mathcal{Q}_q(f) |v|^2 \, \mathrm{d}v = 0. \tag{2.8}$$

Then if one defines the macroscopic quantities: density ρ, average velocity u, specific internal energy e, stress tensor $\mathbb{P}$, and heat flux q as

$$\rho = \int_{\mathbb{R}^d} f \, \mathrm{d}v, \quad \rho u = \int_{\mathbb{R}^d} v f \, \mathrm{d}v, \quad \rho e = \frac{1}{2} \int_{\mathbb{R}^d} |v - u|^2 f \, \mathrm{d}v, \tag{2.9}$$

$$\mathbb{P} = \int_{\mathbb{R}^d} (v - u) \otimes (v - u) f \, \mathrm{d}v, \quad q = \frac{1}{2} \int_{\mathbb{R}^d} (v - u) |v - u|^2 f \, \mathrm{d}v, \tag{2.10}$$

the following local conservation laws can be obtained from Eq. (2.1) after multiplication by $(1, v, |v|/2)^T$ and integration w.r.t. v:

$$\begin{cases} \partial_t \rho + \nabla_x \cdot (\rho u) = 0, \\ \partial_t (\rho u) + \nabla_x \cdot (\rho u \otimes u + \mathbb{P}) = 0, \\ \partial_t \left(\rho e + \frac{1}{2} \rho u^2 \right) + \nabla_x \cdot \left(\left(\rho e + \frac{1}{2} \rho u^2 \right) u + \mathbb{P} u + q \right) = 0. \end{cases} \tag{2.11}$$

2. $\mathcal{Q}_q$ satisfies the Boltzmann's H-theorem:

$$\int_{\mathbb{R}^d} \ln \frac{f}{1 \pm \theta_0 f} \mathcal{Q}_q(f) \, \mathrm{d}v \le 0. \tag{2.12}$$

Moreover, the equality holds iff $\mathcal{Q}_q(f) = 0$ and iff f reaches the local equilibrium—the quantum Maxwellian (also called Bose–Einstein or Fermi–Dirac distribution):

$$\mathcal{M}_q = \frac{1}{\theta_0} \frac{1}{z^{-1} e^{\frac{(v-u)^2}{2T}} \mp 1}. \tag{2.13}$$

[1] Strictly speaking, $\theta_0 = \left(\frac{2\pi\hbar}{m x_0 v_0} \right)^d N$, where m is the particle mass, x_0 and v_0 are the typical values of length and velocity, N is the total number of particles.

The new macroscopic quantities z and T are the fugacity and temperature. They are related to ρ and e via

$$\begin{cases} \rho = \frac{(2\pi T)^{\frac{d}{2}}}{\theta_0} Q_{\frac{d}{2}}(z), \\ e = \frac{d}{2} T \frac{Q_{\frac{d}{2}+1}(z)}{Q_{\frac{d}{2}}(z)}, \end{cases} \tag{2.14}$$

where $Q_\nu(z)$ is the Bose–Einstein/Fermi–Dirac function of order ν [30]:

$$Q_\nu(z) = \frac{1}{\Gamma(\nu)} \int_0^\infty \frac{x^{\nu-1}}{z^{-1}e^x \mp 1} dx, \quad \begin{pmatrix} 0 < z < 1 & \text{for Bose gas} \\ 0 < z < \infty & \text{for Fermi gas} \end{pmatrix}, \tag{2.15}$$

and $\Gamma(\nu) = \int_0^\infty x^{\nu-1} e^{-x}\, \mathrm{d}x$ is the Gamma function.

Remark 2.1

- Compared to the classical Maxwellian:

$$\mathcal{M}_c = \frac{\rho}{(2\pi T)^{\frac{d}{2}}} e^{-\frac{(v-u)^2}{2T}}, \tag{2.16}$$

the quantum Maxwellian $\mathcal{M}_q$ is not a Gaussian function, and z, T depend nonlinearly on ρ and e, the macroscopic quantities that could be readily obtained by taking the moments of f. In fact, it is not difficult to see that when $z \ll 1$, $Q_\nu(z)$ behaves like z. Therefore, in the system (2.14), with ρ and T fixed, we send $\theta_0 \to 0$, and get

$$\frac{\rho}{(2\pi T)^{\frac{d}{2}}} \approx \frac{z}{\theta_0}, \quad e \approx \frac{d}{2} T. \tag{2.17}$$

Since z is very small, one can neglect ∓ 1 in (2.13), which results in

$$\mathcal{M}_q \approx \frac{z}{\theta_0} e^{-\frac{(v-u)^2}{2T}} \approx \frac{\rho}{(2\pi T)^{\frac{d}{2}}} e^{-\frac{(v-u)^2}{2T}} = \mathcal{M}_c. \tag{2.18}$$

On the other hand, if θ_0 is not small, $\mathcal{M}_q$ and $\mathcal{M}_c$ will be quite different from each other. Figure 1 gives a simple illustration of the aforementioned two regimes, which we will refer to as (nearly) classical regime and quantum regime in the following discussion.

- The physical range of interest for a Bose gas is $0 < z \le 1$, where $z = 1$ corresponds to the onset of Bose–Einstein condensation (BEC). To avoid singularity, in this paper we do not consider this extreme case. We refer to [22,23] for some recent results on the construction of numerical methods for the formation of BEC.

2.1 The Euler Limit

Now as the Knudsen number $\varepsilon \to 0$ in Eq. (2.1), based on the discussion above, f is driven to the quantum Maxwellian $\mathcal{M}_q$. Substituting $\mathcal{M}_q$ into (2.10), we see that $\mathbb{P} = \frac{2}{d}\rho e I$ and $q = 0$ (I is the identity matrix). Hence the system (2.11) can be closed and yields the following quantum Euler equations:

$$\begin{cases} \partial_t \rho + \nabla_x \cdot (\rho u) = 0, \\ \partial_t (\rho u) + \nabla_x \cdot \left(\rho u \otimes u + \frac{2}{d}\rho e I\right) = 0, \\ \partial_t \left(\rho e + \frac{1}{2}\rho u^2\right) + \nabla_x \cdot \left(\left(\frac{d+2}{d}\rho e + \frac{1}{2}\rho u^2\right) u\right) = 0. \end{cases} \tag{2.19}$$

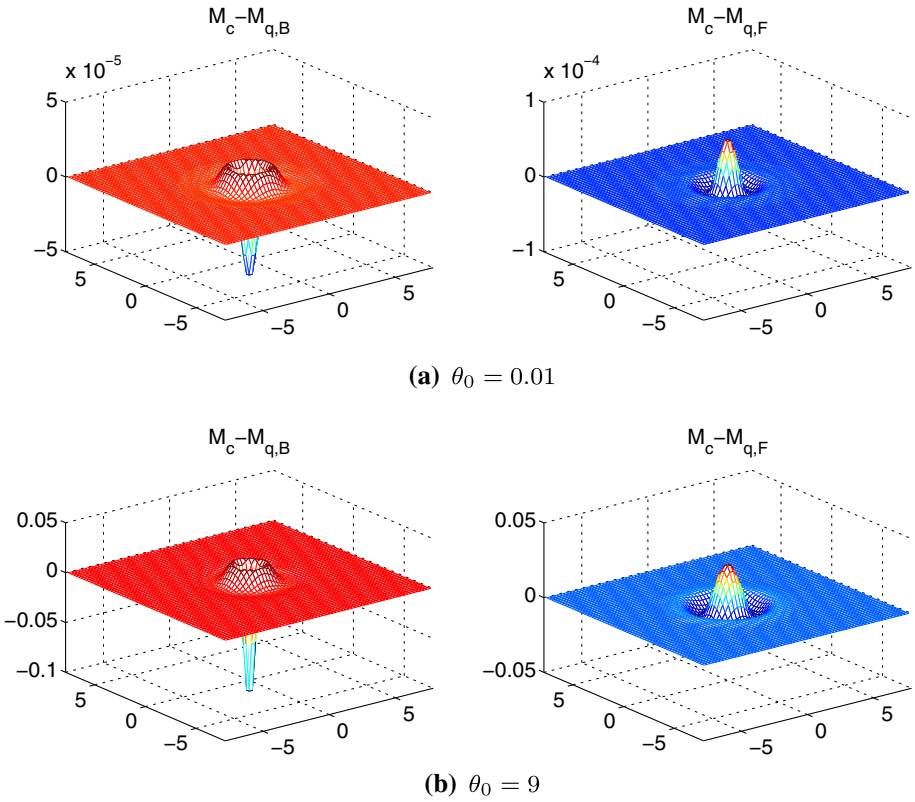

(a) $\theta_0 = 0.01$

(b) $\theta_0 = 9$

Fig. 1 Differences between $\mathcal{M}_c$ and $\mathcal{M}_q$ in **a** the classical regime; **b** the quantum regime. The *left column* is for Bose gas and the *right one* is for Fermi gas

Obviously, written in terms of the macroscopic variables ρ, u, and e, this system is exactly the same as classical Euler equations. The form would be much more complicated if everything is denoted in terms of z, u, and T.

Remark 2.2 By performing a Chapman–Enskog expansion to the next order, one can obtain the quantum Navier–Stokes (NS) system which differs from its classical counterpart [1]. In particular, the viscosity and heat conductivity coefficients not only depend on e but also on ρ. The design of a numerical scheme which is capable to capture with high accuracy the NS limit is actually under study and will be considered in future work.

3 The Asymptotic-Preserving (AP) Exponential Methods

In this section we propose a class of high-order numerical methods for the quantum Boltzmann equation that

- gives accurate solution in both kinetic and fluid regimes, with time discretization not controlled by ε;
- is accurate for both classical and quantum regimes with accuracy analysis independent of θ_0 (or Planck constant $\hbar$).

We want to avoid computing the Eq. (2.1) directly: for numerical stability, if explicit method is used, the time step size should be at most $\mathcal{O}(\varepsilon)$ which poses prohibitive numerical expenses in the fluid regime. On the other hand, implicit method is not feasible due to the complicated collision operator. We need an explicit scheme that relaxes h to be independent of ε but still captures the right asymptotic limit, i.e. to achieve AP property.

To that end, we need to go through two steps: we first rewrite the Eq. (2.1) in an exponential form, and then apply the explicit Runge–Kutta methods on the newly derived equation. The difficulty is two fold: firstly, the equation needs to be reformulated in a way such that explicit Runge–Kutta, under very mild condition, automatically achieves AP property, and secondly, the new terms emerged in the new equation need to be treated with consistent schemes. We address these two difficulties in the following two subsections respectively.

3.1 Reformulation of the Equation and Basic Numerical Methods

In this subsection, we reformulate the Eq. (2.1) in a form such that basic explicit Runge–Kutta methods automatically achieve asymptotic-preserving properties. The idea is adopted from [6,20]:

$$\partial_t \left[(f - \mathcal{M}_q) e^{\frac{\mu t}{\varepsilon}} \right] = \left[\frac{\mathcal{Q}_q(f) - \mu(\mathcal{M}_q - f)}{\varepsilon} - v \cdot \nabla_x f - \partial_t \mathcal{M}_q \right] e^{\frac{\mu t}{\varepsilon}}. \tag{3.1}$$

This equation is derived through simple calculation, and is completely equivalent to the original quantum Boltzmann Eq. (2.1). However, if explicit methods are applied onto this equation instead of the original one, one could obtain the AP property.

In the Eq. (3.1), μ could be any constant independent of time, and $\mathcal{M}_q$ is the local quantum Maxwellian function. As it shares the same moments with f, we update them through the following equation:

$$\partial_t \int \phi \mathcal{M}_q \mathrm{d}v = \partial_t \int \phi f \mathrm{d}v = -\int \phi (v \cdot \nabla_x f) \mathrm{d}v, \quad \phi = (1, v, |v|/2)^T. \tag{3.2}$$

In the derivation we also used the fact that the first $d + 2$ moments of $\mathcal{Q}_q$ are all zeros, as mentioned in (2.8).

Note that to insure the validity of (3.1), μ could be any $\mathcal{O}(1)$ constant independent of time. If positivity is desired, we require:

$$\mu \geq \sup_{v,t} |\mathcal{Q}_q^-|, \tag{3.3}$$

where $\mathcal{Q}_q^-$ is the loss part of the collision operator (2.4).

We then apply the standard Runge–Kutta method to Eqs. (3.1) and (3.2). The simplest example is the forward Euler scheme:

$$\begin{cases} (f^{n+1} - \mathcal{M}_q^{n+1}) e^{\lambda} = (f^n - \mathcal{M}_q^n) + \frac{h}{\varepsilon} \left[P^n - \mu \mathcal{M}_q^n - \varepsilon v \cdot \nabla_x f^n - \varepsilon \partial_t \mathcal{M}_q^n \right], \\ \int \phi \mathcal{M}_q^{n+1} \mathrm{d}v = \int \phi f^{n+1} \mathrm{d}v = \int \phi f^n \mathrm{d}v - h \int \phi (v \cdot \nabla_x f^n) \mathrm{d}v, \end{cases} \tag{3.4}$$

where h is the time step, $\lambda = \mu h / \varepsilon$, and the operator P is defined as $P(f) = \mathcal{Q}_q(f) + \mu f$. The more general κ-step explicit Runge–Kutta method gives:

- Stage i $(i = 1, \ldots, \kappa)$:

$$\begin{cases} (f^{(i)} - \mathcal{M}_q^{(i)}) e^{c_i \lambda} = (f^n - \mathcal{M}_q^n) + \sum_{j=1}^{i-1} a_{ij} \frac{h}{\varepsilon} \\ \qquad \left[P^{(j)} - \mu \mathcal{M}_q^{(j)} - \varepsilon v \cdot \nabla_x f^{(j)} - \varepsilon \partial_t \mathcal{M}_q^{(j)} \right] e^{c_j \lambda}, \\ \int \phi \mathcal{M}_q^{(i)} \mathrm{d}v = \int \phi f^{(i)} \mathrm{d}v = \int \phi f^n \mathrm{d}v + \sum_{j=1}^{i-1} a_{ij} \left(-h \int \phi v \cdot \nabla_x f^{(j)} \mathrm{d}v \right); \end{cases} \tag{3.5a}$$

- Final Stage:

$$\begin{cases} (f^{n+1} - \mathcal{M}_q^{n+1})e^{\lambda} = (f^n - \mathcal{M}_q^n) + \sum_{i=1}^{\kappa} b_i \frac{h}{\varepsilon} \\ \qquad\qquad \left[P^{(i)} - \mu \mathcal{M}_q^{(i)} - \varepsilon v \cdot \nabla_x f^{(i)} - \varepsilon \partial_t \mathcal{M}_q^{(i)}\right] e^{c_i \lambda}, \\ \int \phi \mathcal{M}_q^{n+1} \mathrm{d}v = \int \phi f^{n+1} \mathrm{d}v = \int \phi f^n \mathrm{d}v + \sum_{i=1}^{\kappa} b_i \left(-h \int \phi v \cdot \nabla_x f^{(i)} \mathrm{d}v\right), \end{cases} \tag{3.5b}$$

where $f^{(i)}$ stands for the estimation of f at time $t = t^n + c_i h$. a_{ij}, b_i, and c_i are Runge–Kutta coefficients that satisfy $\sum_{j=1}^{i-1} a_{ij} = c_i$ and $\sum_{i=1}^{\kappa} b_i = 1$. They are usually stored in a Butcher tableau as:

$$\begin{array}{c|c} c & A \\ \hline & b^T \end{array} \tag{3.6}$$

Clearly at each stage i, to evaluate $f^{(i)}$, one needs to find $\mathcal{M}_q^{(i)}$ at the new stage first, and a good approximation of $\partial_t \mathcal{M}_q^{(j)}$ at old stages (this also applies to the final stage).

Before moving to the next step some considerations are necessary.

Remark 3.1
- The above exponential approach applied to Eq. (3.1) corresponds to the so-called integrating factor method [13]. Here we limit our analysis to this class of schemes, however, we refer to [10,13,20] for other possible exponential techniques that can be used to construct other types of AP exponential schemes.
- Reformulation (3.1) holds true for arbitrary function $\mathcal{M}_q$ which shares the same moments with f. We use the local Maxwellian $\mathcal{M}_q$ because this guarantees the strong AP property, as will be proved in Sect. 4. A simplifying assumption, analyzed in [20], consists in taking $\mathcal{M}_q$ constant along the time stepping so that the term $\partial_t \mathcal{M}_q$ disappears and the scheme simplifies. This choice, although in general less accurate in intermediate regimes, permits to obtain AP schemes with better stability and monotonicity properties. We leave the analysis of this approach in the quantum case for future studies and refer to [20] for further details.

3.2 Computation of $\mathcal{M}_q^{(i)}$ and $\partial_t \mathcal{M}_q^{(j)}$

We now show how to evaluate $\mathcal{M}_q^{(i)}$ and $\partial_t \mathcal{M}_q^{(j)}$ provided $f^{(j)}$, $\mathcal{M}_q^{(j)}$ ($j < i$) are known from previous stages.

– Computation of $\mathcal{M}_q^{(i)}$.

By definition in (2.13), $\mathcal{M}_q^{(i)}$ is obtained once we have $u^{(i)}$, $z^{(i)}$, and $T^{(i)}$. The second equation in (3.5a) gives the macroscopic quantities $\rho^{(i)}$, $u^{(i)}$, and $e^{(i)}$, and thus to obtain $z^{(i)}$ and $T^{(i)}$, one only needs to invert the system (2.14). Note that the 2×2 system is nonlinear. In the implementation, we use the standard Newton-iteration. Details about the approximation and inversion of the quantum function $Q_\nu(z)$ can be found in [14].

– Computation of $\partial_t \mathcal{M}_q^{(j)}$.

This is the key idea of the scheme. Write $\mathcal{M}_q = \mathcal{M}_q(z, T, u)$, it is not difficult to derive that (we drop the superscript (j) for simplicity)

$$\partial_t \mathcal{M}_q = \mathcal{M}_q(1 \pm \theta_0 \mathcal{M}_q) \left[\frac{1}{z} \partial_t z + \frac{(v-u)^2}{2T^2} \partial_t T + \frac{v-u}{T} \cdot \partial_t u\right]. \tag{3.7}$$

While $\partial_t \rho$, $\partial_t u$, and $\partial_t e$ can be directly obtained from the macroscopic equations as we shall see, the computation of $\partial_t z$ and $\partial_t T$ is, however, not explicit. Therefore, it is desirable to

transform the expression (3.7) in terms of $\partial_t \rho$, $\partial_t u$, and $\partial_t e$. Through the straightforward but cumbersome calculations in the Appendix, we end up with:

$$\partial_t \mathcal{M}_q = \mathcal{M}_q (1 \pm \theta_0 \mathcal{M}_q) \left[A \partial_t \rho + B \partial_t e + C \cdot \partial_t u \right], \tag{3.8}$$

where

$$A = \frac{1}{\rho} \left(M(z) + \frac{(v-u)^2}{dT} (1 - N(z)) \right), \tag{3.9}$$

$$B = \left(\frac{(v-u)^2}{2eT} N(z) - \frac{d}{2e} M(z) \right), \tag{3.10}$$

$$C = \frac{v-u}{T}, \tag{3.11}$$

and $M(z)$ and $N(z)$ are defined by:

$$M(z) = \frac{Q_{\frac{d}{2}}(z)}{\left(\frac{d}{2}+1\right) Q_{\frac{d}{2}-1}(z) - \frac{d^2 T}{4e} Q_{\frac{d}{2}}(z)}, \quad N(z) = \frac{Q_{\frac{d}{2}-1}(z)}{\left(\frac{d}{2}+1\right) Q_{\frac{d}{2}-1}(z) - \frac{d^2 T}{4e} Q_{\frac{d}{2}}(z)}. \tag{3.12}$$

To compute $\partial_t \rho$, $\partial_t u$, and $\partial_t e$, we use Eq. (3.2) to transform the time derivative into spatial derivative, namely:

$$\begin{cases} \partial_t \rho = \partial_t \int \mathcal{M}_q \mathrm{d}v = -\int v \cdot \nabla_x f \mathrm{d}v := -F_1, \\ \partial_t (\rho u) = \partial_t \int v \mathcal{M}_q \mathrm{d}v = -\int v (v \cdot \nabla_x f) \mathrm{d}v := -F_2, \\ \partial_t \left(\rho e + \frac{1}{2} \rho u^2 \right) = \partial_t \int \frac{v^2}{2} \mathcal{M}_q \mathrm{d}v = -\int \frac{v^2}{2} (v \cdot \nabla_x f) \mathrm{d}v := -F_3, \end{cases} \tag{3.13}$$

which is

$$\begin{cases} \partial_t \rho = -F_1, \\ \partial_t u = \frac{1}{\rho} (-F_2 + F_1 u), \\ \partial_t e = \frac{1}{\rho} \left(-F_3 + F_1 e + \frac{1}{2} F_1 u^2 + u \cdot (F_2 - F_1 u) \right). \end{cases} \tag{3.14}$$

In this way, we could compute the time derivatives using only spatial discretizations, and the scheme is automatically consistent with the framework (3.5).

4 Properties of the Exponential AP Methods

In this section we briefly analyze the numerical scheme. We are going to show that our scheme is consistent, recovers the classical Boltzmann equation in the classical regime, and is AP. The choice (3.3) of μ guarantees the positivity, and the proof was given in section 4.1 of [20]. We omit it here.

1. The classical regime:

In the classical regime, θ_0 (or the Planck constant) is considered as a very small number, and the fugacity $z \to 0$. In this regime, theoretically, the quantum Boltzmann equation recovers the classical Boltzmann equation, and our schemes should reflect this consistency. For $z \ll 1$, as we have seen previously $Q_\nu(z) \approx z$, and $e \approx \frac{d}{2} T$. By definition, $M(z), N(z) \approx 1$. Plugging these relations back into

- equation (3.8): we have

$$A \approx \frac{1}{\rho}, \quad B \approx \frac{(v-u)^2}{2eT} - \frac{d}{2e}, \quad C = \frac{v-u}{T}. \tag{4.1}$$

Therefore,

$$\partial_t \mathcal{M}_q \approx \mathcal{M}_q \left[\frac{1}{\rho}\partial_t \rho + \left(\frac{d}{4e^2}(v-u)^2 - \frac{d}{2e} \right) \partial_t e + \frac{d}{2e}(v-u)\cdot \partial_t u \right]. \tag{4.2}$$

This is indeed the time evolution of the classical Maxwellian function $\partial_t \mathcal{M}_c$;

- equation (2.13): as argued in Remark 2.1, $\mathcal{M}_q$ goes to $\mathcal{M}_c$;
- equation (2.2): formally $\mathcal{Q}_q$ also becomes the classical collision operator $\mathcal{Q}_c$ as $\theta_0 \to 0$.

Combining these three arguments, we see that the scheme (3.5) becomes the Exponential AP method developed for the classical Boltzmann equation in [20]. We successfully recovers the classical regime.

2. Consistency:
Here we assume the time step h resolves ε. We firstly rewrite the scheme (3.5a) as:

$$\begin{aligned} f^{(i)} &= \mathcal{M}_q^{(i)} + (f^n - \mathcal{M}_q^n) e^{-c_i \lambda} \\ &\quad + \sum_j a_{ij} \frac{h}{\varepsilon} \left[P^{(j)} - \mu \mathcal{M}_q^{(j)} - \varepsilon v \cdot \nabla_x f^{(j)} - \varepsilon \partial_t \mathcal{M}_q^{(j)} \right] e^{(c_j - c_i)\lambda}. \end{aligned} \tag{4.3}$$

As h is small, we Taylor expand the exponential term, and rewrite $e^{-c_i\lambda} \sim 1 - c_i\lambda$ and $e^{(c_j-c_i)\lambda} \sim 1 + (c_j - c_i)\lambda$. We keep $\mathcal{O}(1)$ and $\mathcal{O}(h)$ terms and neglect higher orders, the scheme becomes:

$$f^{(i)} = \Lambda_1 + \Lambda_h + \mathcal{O}(h^2), \tag{4.4}$$

with

$$\Lambda_1 = \mathcal{M}_q^{(i)} + f^n - \mathcal{M}_q^n; \tag{4.5}$$

$$\Lambda_h = -c_i\lambda(f^n - \mathcal{M}_q^n) + \sum_j a_{ij} \frac{h}{\varepsilon} \left[P^{(j)} - \mu \mathcal{M}_q^{(j)} - \varepsilon v \cdot \nabla_x f^{(j)} - \varepsilon \partial_t \mathcal{M}_q^{(j)} \right]. \tag{4.6}$$

As $\mathcal{M}_q^{(i)}$ is the Maxwellian obtained with macroscopic quantities evaluated at time $t^n + c_i h$, and thus the difference $\mathcal{M}_q^{(i)} - \mathcal{M}_q^n$ is at most order h, therefore, one has

$$\Lambda_1 = f^n + c_i h \partial_t \mathcal{M}_q^n + \mathcal{O}(h^2). \tag{4.7}$$

On the other hand, we rewrite Λ_h as:

$$\begin{aligned} \Lambda_h &= \sum_j a_{ij} h \left(\frac{Q^{(j)}}{\varepsilon} - v \cdot \nabla_x f^{(j)} \right) \\ &\quad + \sum_j a_{ij} \lambda (f^{(j)} - \mathcal{M}_q^{(j)}) - c_i \lambda (f^n - \mathcal{M}_q^n) - \sum_j a_{ij} h \partial_t \mathcal{M}_q^{(j)}. \end{aligned}$$

As $f^{(j)} - f^n = \mathcal{O}(h)$, $\mathcal{M}_q^{(j)} - \mathcal{M}_q^n = \mathcal{O}(h)$, and $\sum_j a_{ij} = c_i$, we rewrite it as:

$$\Lambda_h = \sum_j a_{ij} h \left(\frac{Q^{(j)}}{\varepsilon} - v \cdot \nabla_x f^{(j)} \right) - c_i h \partial_t \mathcal{M}_q^n + \mathcal{O}(h^2). \tag{4.8}$$

Combining Eqs. (4.7) and (4.8), we have

$$f^{(i)} = f^n + h \sum_j a_{ij} \left(\frac{Q^{(j)}}{\varepsilon} - v \cdot \nabla_x f^{(j)} \right) + \mathcal{O}(h^2), \tag{4.9}$$

and the consistency of the scheme is obvious. We could perform the same analysis to (3.5b) and the proof will be omitted from here.

3. Asymptotic preserving:
Here we show AP property of the numerical scheme, namely, as $\varepsilon \to 0$, the distribution function will automatically capture the solution to the Euler equation. For simplicity, we only show proof for the case when $0 \le c_1 < c_2 < \cdots < c_\kappa < 1$. The argument presented here will no longer hold if any sub-stage share the same time step, i.e. $c_i = c_{i+1}$ for some i, but we still have the same conclusion. The proof for that more general case could be found in [20].
We still use the formula (4.3). As c_i monotonically increases, in the zero limit of $\varepsilon, \lambda \to \infty$ and the second and the third terms in (4.3) vanish, leaving:

$$f^{(i)} = \mathcal{M}_q^{(i)} + \mathcal{O}\left(\lambda e^{-c\lambda}\right) \sim \mathcal{M}_q^{(i)}, \quad i = 1, \ldots, \kappa,$$

with $c = \min_i |c_{i+1} - c_i| > 0$. We take the moment of both sides, and combine it with the second equation in the scheme (3.5a):

$$\int \phi f^{(i)} \mathrm{d}v \sim \int \phi f^n \mathrm{d}v - \sum_j a_{ij} h \int \phi v \cdot \nabla_x \mathcal{M}_q^{(j)} \mathrm{d}v. \tag{4.10}$$

Similarly for the numerical solution from (3.5b) we obtain

$$\int \phi f^{n+1} \mathrm{d}v \sim \int \phi f^n \mathrm{d}v - \sum_i b_i h \int \phi v \cdot \nabla_x \mathcal{M}_q^{(i)} \mathrm{d}v. \tag{4.11}$$

This is exactly how we close the moment system and obtain the Euler equation analytically, and thus we capture the Euler limit. Let us note that the limiting resulting scheme (4.10)–(4.11) is nothing but the underlying explicit Runge–Kutta method, used in the construction of the exponential scheme, applied to the limiting Euler system. Therefore the method is not only consistent but it preserves the order of accuracy in the fluid limit.

5 Numerical Examples

In this section we present several numerical results using our schemes. The first example is to show the AP property. The reference solution is given by directly applying the forward Euler method on (2.1). In this case, for stability reason, time step h has to be small, and controlled by ε. In comparison, h only needs to satisfy the CFL condition in our method. The second example verifies the high-order accuracy. The value μ in all examples is chosen as $\mu = 0.1$. Note that both examples are performed for x in 1D and v in 2D. Exp-RK2 is referred to as RK2 in time coupled with second-order Lax-Wendroff scheme with van Leer

limiter in space [19]. Exp-RK3 is referred to as RK3 in time coupled with standard WENO3 in space [32]. The Butcher tableaux of RK2 (midpoint) and RK3 (Heun method [12]) we used in computation are given as follows:

$$\begin{array}{c|cc} 0 & 0 & 0 \\ 1/2 & 1/2 & 0 \\ \hline & 0 & 1 \end{array} \qquad \begin{array}{c|ccc} 0 & 0 & 0 & 0 \\ 1/3 & 1/3 & 0 & 0 \\ 2/3 & 0 & 2/3 & 0 \\ \hline & 1/4 & 0 & 3/4 \end{array} \tag{5.1}$$

For the velocity discretization, we use 64 points in each direction and perform the fast spectral method [16] for Maxwell molecule kernels. We use $v_{\max} = 7.86$, which is determined by the criteria of the spectral method for the collision operator [25]. If our AP scheme is used, time step is chosen to satisfy the CFL condition $v_{\max}\frac{h}{\Delta x} \approx 0.5$. Furthermore, functions $M(z)$ and $N(z)$ (in the evaluation of $\partial_t \mathcal{M}_q$) have the following simple form when $d = 2$:

$$M(z) = \frac{Q_1(z)}{2Q_0(z) - \frac{T}{e}Q_1(z)}, \quad N(z) = \frac{Q_0(z)}{2Q_0(z) - \frac{T}{e}Q_1(z)}, \tag{5.2}$$

where for

- Bose gas: $Q_1(z) = -\ln(1-z)$, $Q_0(z) = \frac{z}{1-z}$;
- Fermi gas: $Q_1(z) = \ln(1+z)$, $Q_0(z) = \frac{z}{1+z}$.

5.1 Sod Problem

In this subsection we compute a Sod problem. In this problem, in the limiting Euler regime, the solution should have a shock, a rarefaction and a contact discontinuity. The initial data for the macroscopic quantities are chosen as:

$$\begin{cases} \rho = 1, \quad u_x = 0, \quad u_y = 0, \quad T = 1; \\ \rho = 0.125, \quad u_x = 0, \quad u_y = 0, \quad T = 0.25. \end{cases} \tag{5.3}$$

For the microscopic quantities, we choose $f(t = 0)$ to be a summation of two Gaussians, as shown in Fig. 2, and thus is far away from the quantum equilibrium. Figures 3 and 4 show the numerical results using our new schemes. We consider both classical regime ($\theta_0 = 0.01$) and quantum regime ($\theta_0 = 9$) (the behaviors of Bose gas and Fermi gas in the classical regime are very close to the classical gas, thus one of them is omitted). In the case when Knudsen $\varepsilon = 0.01$ (kinetic regime), the reference solutions are given by directly applying the forward Euler scheme onto the original Boltzmann equation with the spacial discretization $\Delta x = 1/160$, and time step $h = 1/2{,}560$, and our method uses $\Delta x = 1/80$ and $h = 1/1{,}280$. When $\varepsilon = 10^{-6}$ (fluid regime), for reference data, we could not afford the fine discretization any longer since an explicit scheme would require $h = \mathcal{O}(10^{-6})$, and thus we directly compute the limiting Euler equation. In contrast, our new scheme only uses $\Delta x = 1/160$ and $h = 1/2{,}560 \approx \mathcal{O}(10^{-4})$, much bigger than the Knudsen number ε. We also measured the difference between the distribution function f and the Maxwellian $\mathcal{M}_q$. In Fig. 5 we can clearly see that smaller ε gives faster convergence towards the Maxwellian.

For comparison, we mention that the same initial data (5.3) was used in [8] for testing the first-order IMEX AP scheme. The results we obtained here are very similar to those but with better resolution (due to the higher-order accuracy of the scheme).

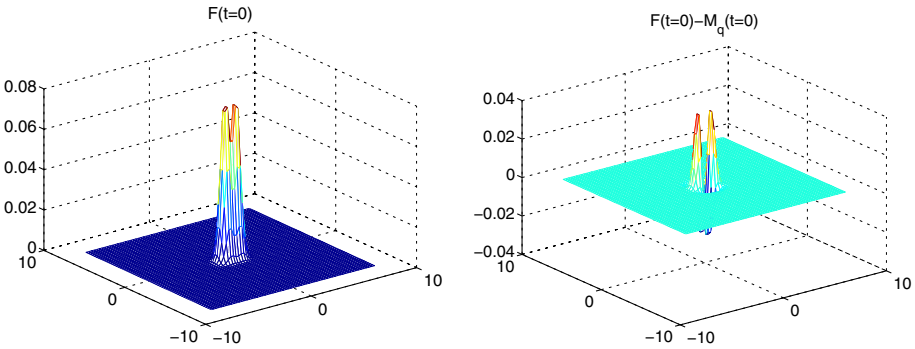

Fig. 2 Sod problem. The initial distribution at $x = -1$. The figure on *left* is $f(t = 0)$ and *right* is $f - \mathcal{M}_q$

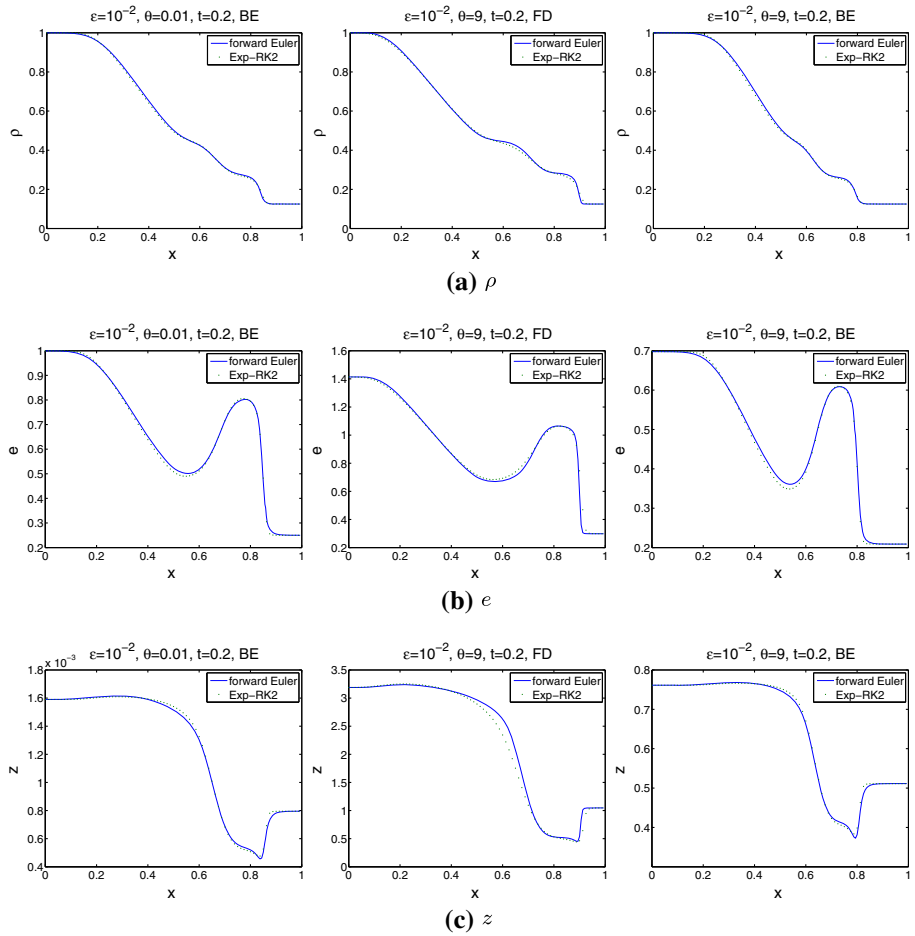

(a) ρ

(b) e

(c) z

Fig. 3 Sod problem. $\varepsilon = 10^{-2}$ (kinetic regime). The three columns, from the *left* to the *right* are for Bose gas in classical regime, Fermi gas in quantum regime and Bose gas in quantum regime. The three rows present density ρ, internal energy e and fugacity z. Note the scale differences for the three cases

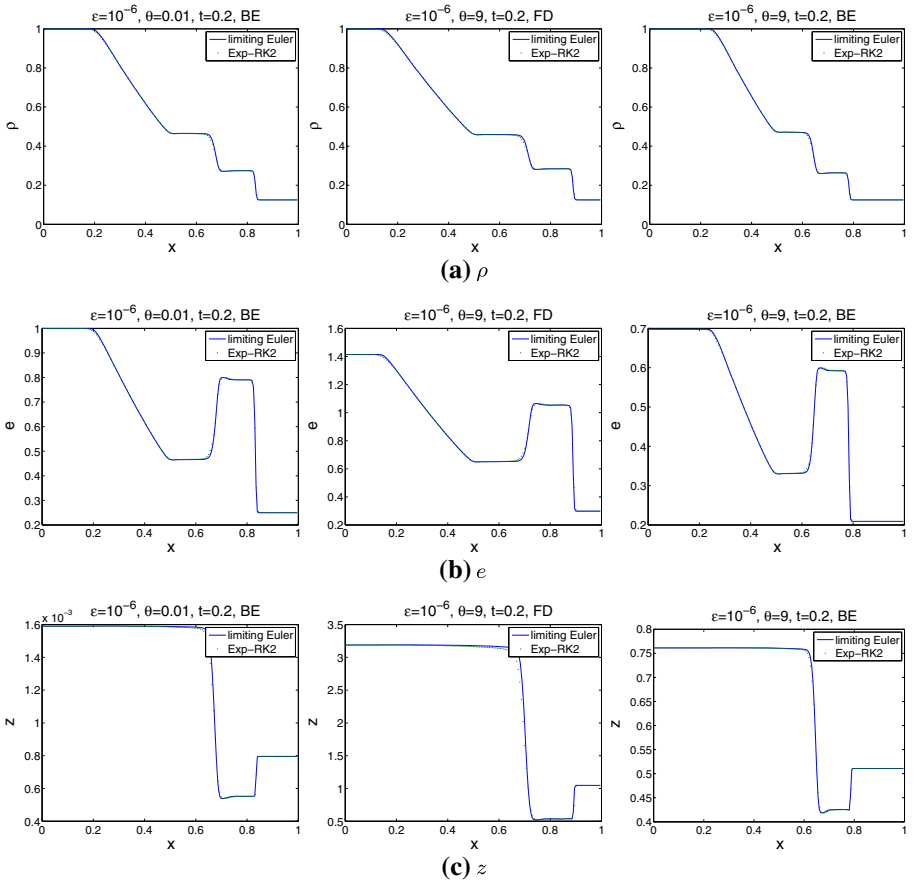

Fig. 4 Sod problem. $\varepsilon = 10^{-6}$ (fluid regime). The three columns, from the *left* to the *right* are for Bose gas in classical regime, Fermi gas in quantum regime and Bose gas in quantum regime. The three rows present density ρ, internal energy e and fugacity z. Note the scale differences for the three cases

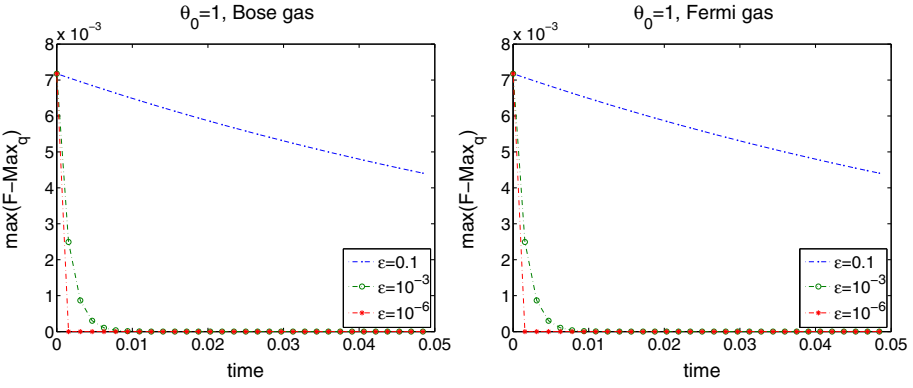

Fig. 5 Sod problem. The difference between the distribution function f and the Maxwellian $\mathcal{M}_q$ decays in time. The figure on the *left* is for Bose gas and the *right one* is for Fermi gas. $\theta_0 = 1$

5.2 Convergence Rate Test

In the second example we show the convergence rate. We use the following smooth initial data:

$$\begin{cases} \rho = 0.3125 + 0.1875\cos(2\pi x); \\ e = 0.625 + 0.375\cos(2\pi x); \\ u_x = u_y = 0; \end{cases} \tag{5.4}$$

h is chosen such that the CFL number is 0.5 (independent of ε). Note that this is the unique stability restriction that we must impose in our numerical discretization.

To measure the convergence rate, we check the L_1 error of ρ and compute the decay rate using:

$$\text{Error}_i = \max_{t=t^n} \frac{\|\rho_i(t) - \rho_{i-1}(t)\|_1}{\|\rho_{i-1}(t)\|_1}. \tag{5.5}$$

Here the notation ρ_i is ρ computed on $2^i \times 20$ (with i being a integer) grid points. Theoretically, if a numerical scheme is of k-th order, then the error should decay as: $\text{Error}_i < C\,(i)^{-k}$ for h small enough.

In each subfigure in Fig. 6, we show the convergence rate with $\theta_0 = 1$ and $\theta_0 = 10^{-2}$ using Exp-RK2 and Exp-RK3. We perform the same test for both Bose gas and Fermi gas in both kinetic regime and fluid regime. The numerical results are in good agreement with our theoretical expectation.

5.3 Mixing Regime

In the last example, we show the numerical results for a problem with mixing regime. This example is adopted from [15]. We consider the initial data at equilibrium with macroscopic quantities:

$$\begin{cases} \rho = \frac{\sin(2\pi x)+2}{3}, \\ T = \frac{\cos(2\pi x)+3}{4}, \\ u_x = u_y = 0. \end{cases} \tag{5.6}$$

We compute the Fermi gas with $\theta_0 = 2.25$. The problem has mixing regime, and ε varies across kinetic and fluid regimes:

$$\varepsilon = \varepsilon_0 + 0.05\tanh(5 - 10x) + 0.05\tanh(5 + 10x) \tag{5.7}$$

with $\varepsilon_0 = 10^{-3}$. Figure 7 shows the profile of the Knudsen number ε. This problem is difficult if the standard method is applied: the time step is controlled by the smallest Knudsen number although in most part of the domain, the problem is in kinetic regime and time step could have been larger. The AP method we presented here, on the other hand, does not rely on any time constraint beside the CFL condition. In Fig. 8 we show the numerical results given by our method. We used $\Delta x = 1/40$, and $h = 1/640$, and this discretization is bigger than ε_0. The reference solution is computed through explicit method with denser mesh: $\Delta x = 1/160$, and the time discretization resolves ε_0: $h = 1/51{,}200$. We observe good agreement in all quantities. As the purpose here is show the effectiveness of the AP scheme, but not the solver for collision operator, to save the computational cost (especially for the explicit method), the computation in velocity space was done using the quantum BGK model.

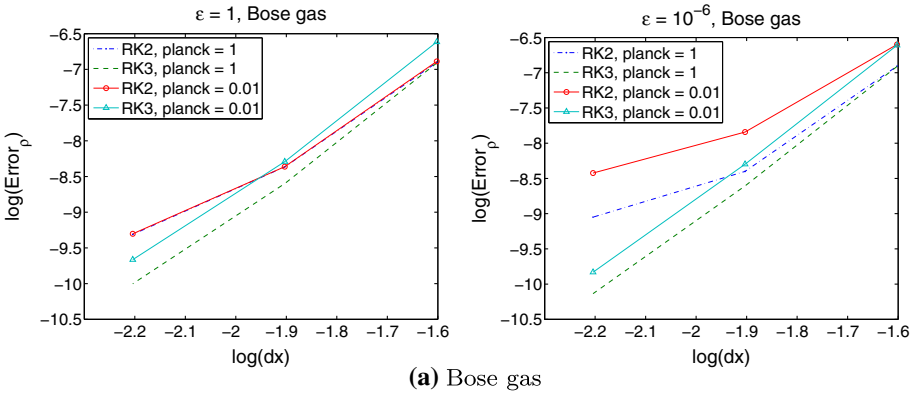

(a) Bose gas

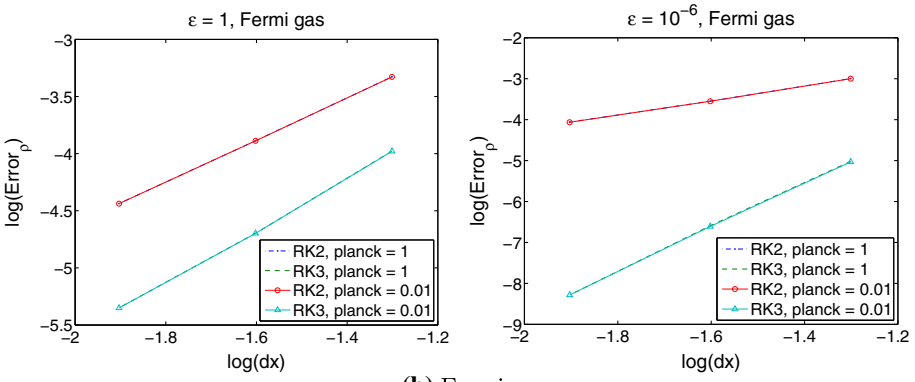

(b) Fermi gas

Fig. 6 Convergence rate test. The *left column* is for $\varepsilon = 1$ and $\varepsilon = 10^{-6}$ on the *right*. The *top figures* are for Bose gas and the *bottom ones* are for Fermi gas

Fig. 7 Mixing regime: the Knudsen number varies across regimes

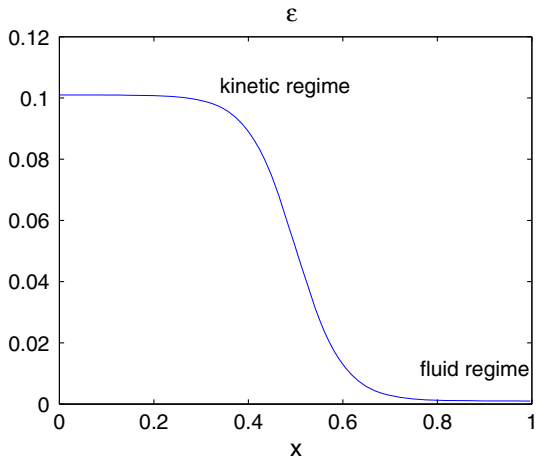

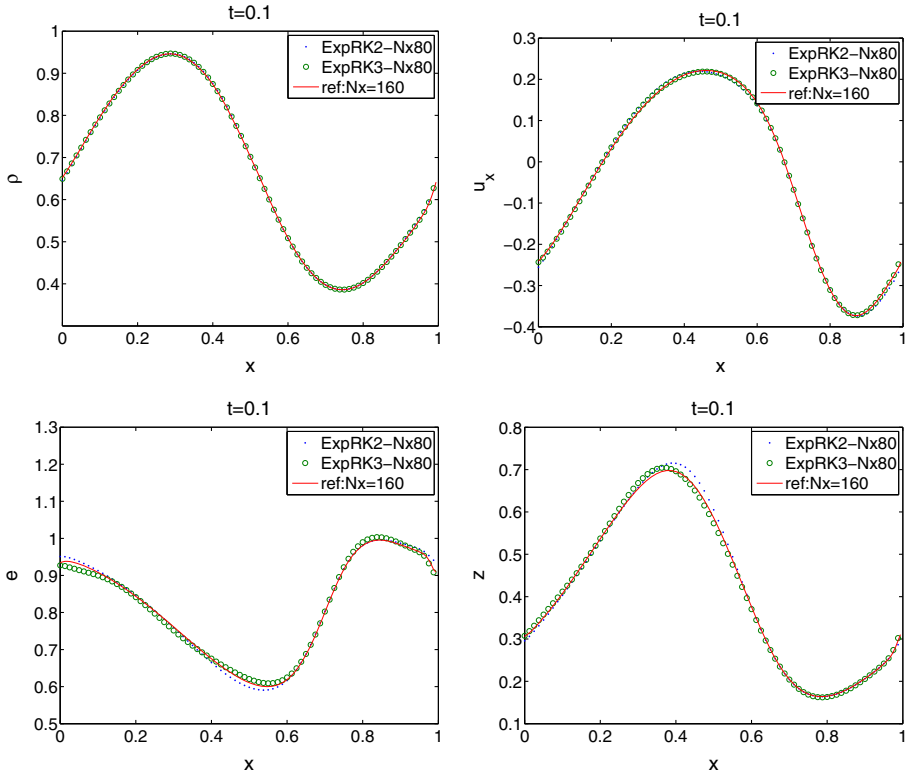

Fig. 8 Mixing regime. *Top*: density ρ and velocity u_x; *bottom*: internal energy e and fugacity z

6 Conclusions

In this paper we have extended the numerical approach recently introduced in [20] to the case of the quantum Boltzmann equation. In particular, we have shown how to derive high-order asymptotic preserving schemes which work uniformly with respect to the Planck constant. Numerical results for second and third order methods confirm the robustness and accuracy of the present method. We did not tackle the issue of the formation of the Bose–Einstein condensate since this involves also a careful choice of the velocity discretization whereas here we concentrate our attention on the time discretization problem only. In our future research we will focus on these challenging aspects.

Acknowledgments We would like to express our gratitude to the NSF Grant RNMS11-07444 (KI-Net), and CSCAMM, University of Maryland for holding the conference "Quantum Systems: A Mathematical Journey from Few to Many Particles" in May 2013, during which this work was initiated.

7 Appendix: Derivation of $\partial_t \mathcal{M}_q$

In this appendix, we give the details of the derivation of (3.8). Our goal is to represent $\partial_t z$ and $\partial_t T$ in Eq. (3.7) in terms of $\partial_t \rho$ and $\partial_t e$.

First, combining the two equations in system (2.14) gives

$$\frac{Q_{\frac{d}{2}}^{\frac{d}{2}+1}(z)}{Q_{\frac{d}{2}+1}^{\frac{d}{2}}(z)} = \theta_0 \left(\frac{d}{4\pi e}\right)^{\frac{d}{2}} \rho. \tag{7.1}$$

Therefore, we define a function $F(z)$ such that

$$y = F(z) = \frac{Q_{\frac{d}{2}}^{\frac{d}{2}+1}(z)}{Q_{\frac{d}{2}+1}^{\frac{d}{2}}(z)}, \tag{7.2}$$

and a function $G(y)$ such that

$$z = G(y) = F^{-1}(y). \tag{7.3}$$

Then we have

$$G'(y) = \frac{1}{F'(z)} = \frac{Q_{\frac{d}{2}+1}^{d}(z)}{\left(\frac{d}{2}+1\right) Q_{\frac{d}{2}}^{\frac{d}{2}}(z) Q'_{\frac{d}{2}}(z) Q_{\frac{d}{2}+1}^{\frac{d}{2}}(z) - \frac{d}{2} Q_{\frac{d}{2}+1}^{\frac{d}{2}-1}(z) Q'_{\frac{d}{2}+1}(z) Q_{\frac{d}{2}}^{\frac{d}{2}+1}(z)}. \tag{7.4}$$

For the Bose–Einstein/Fermi–Dirac function, one has the following nice property (see [30])

$$z Q'_{\nu}(z) = Q_{\nu-1}(z). \tag{7.5}$$

Using (7.5) in (7.4),

$$\begin{aligned} G'(y) = \frac{1}{F'(z)} &= \frac{z Q_{\frac{d}{2}+1}^{d}(z)}{\left(\frac{d}{2}+1\right) Q_{\frac{d}{2}}^{\frac{d}{2}}(z) Q_{\frac{d}{2}-1}(z) Q_{\frac{d}{2}+1}^{\frac{d}{2}}(z) - \frac{d}{2} Q_{\frac{d}{2}+1}^{\frac{d}{2}-1}(z) Q_{\frac{d}{2}}(z) Q_{\frac{d}{2}}^{\frac{d}{2}+1}(z)} \\ &= \frac{z Q_{\frac{d}{2}+1}^{\frac{d}{2}+1}(z)}{Q_{\frac{d}{2}}^{\frac{d}{2}}(z) \left[\left(\frac{d}{2}+1\right) Q_{\frac{d}{2}-1}(z) Q_{\frac{d}{2}+1}(z) - \frac{d}{2} Q_{\frac{d}{2}}^{2}(z)\right]}. \end{aligned} \tag{7.6}$$

From the second equation of (2.14) we know

$$Q_{\frac{d}{2}+1}(z) = \frac{2e}{dT} Q_{\frac{d}{2}}(z), \tag{7.7}$$

then

$$G'(y) = \frac{z \left(\frac{2e}{dT}\right)^{\frac{d}{2}}}{\left(\frac{d}{2}+1\right) Q_{\frac{d}{2}-1}(z) - \frac{d^2 T}{4e} Q_{\frac{d}{2}}(z)}. \tag{7.8}$$

Note that

$$z = G\left(\theta_0 \left(\frac{d}{4\pi e}\right)^{\frac{d}{2}} \rho\right), \quad T = \frac{\theta_0^{\frac{2}{d}}}{2\pi} \left(\frac{\rho}{Q_{\frac{d}{2}}(z)}\right)^{\frac{2}{d}}, \tag{7.9}$$

so we have

$$\partial_t z = G'\left(\theta_0\left(\frac{d}{4\pi e}\right)^{\frac{d}{2}}\rho\right)\theta_0\left(\frac{d}{4\pi}\right)^{\frac{d}{2}}\left(\frac{1}{e^{\frac{d}{2}}}\partial_t\rho - \frac{d}{2}\frac{\rho}{e^{\frac{d}{2}+1}}\partial_t e\right)$$
$$= \frac{zQ_{\frac{d}{2}}(z)}{\left(\frac{d}{2}+1\right)Q_{\frac{d}{2}-1}(z) - \frac{d^2T}{4e}Q_{\frac{d}{2}}(z)}\left(\frac{1}{\rho}\partial_t\rho - \frac{d}{2e}\partial_t e\right), \tag{7.10}$$

and

$$\partial_t T = \frac{\theta_0^{\frac{2}{d}}}{\pi d}\left(\frac{\rho^{\frac{2}{d}-1}}{Q^{\frac{2}{d}}_{\frac{d}{2}}(z)}\partial_t\rho - \frac{\rho^{\frac{2}{d}}Q'_{\frac{d}{2}}(z)}{Q^{\frac{2}{d}+1}_{\frac{d}{2}}(z)}\partial_t z\right) = \frac{\theta_0^{\frac{2}{d}}}{\pi d}\left(\frac{\rho^{\frac{2}{d}-1}}{Q^{\frac{2}{d}}_{\frac{d}{2}}(z)}\partial_t\rho - \frac{\rho^{\frac{2}{d}}Q_{\frac{d}{2}-1}(z)}{zQ^{\frac{2}{d}+1}_{\frac{d}{2}}(z)}\partial_t z\right)$$
$$= \frac{2T}{d}\frac{1}{\rho}\rho_t - \frac{2T}{d}\frac{Q_{\frac{d}{2}-1}(z)}{Q_{\frac{d}{2}}(z)}\frac{1}{z}\partial_t z = \frac{2T}{d}\frac{1}{\rho}\rho_t$$
$$-\frac{2T}{d}\frac{Q_{\frac{d}{2}-1}(z)}{\left(\frac{d}{2}+1\right)Q_{\frac{d}{2}-1}(z) - \frac{d^2T}{4e}Q_{\frac{d}{2}}(z)}\left(\frac{1}{\rho}\partial_t\rho - \frac{d}{2e}\partial_t e\right). \tag{7.11}$$

Therefore,

$$\frac{1}{z}\partial_t z + \frac{(v-u)^2}{2T^2}\partial_t T = \frac{Q_{\frac{d}{2}}(z)}{\left(\frac{d}{2}+1\right)Q_{\frac{d}{2}-1}(z) - \frac{d^2T}{4e}Q_{\frac{d}{2}}(z)}\left(\frac{1}{\rho}\partial_t\rho - \frac{d}{2e}e_t\right)$$
$$+\frac{(v-u)^2}{dT}\frac{1}{\rho}\partial_t\rho - \frac{(v-u)^2}{dT}\frac{Q_{\frac{d}{2}-1}(z)}{\left(\frac{d}{2}+1\right)Q_{\frac{d}{2}-1}(z) - \frac{d^2T}{4e}Q_{\frac{d}{2}}(z)}\left(\frac{1}{\rho}\partial_t\rho - \frac{d}{2e}\partial_t e\right)$$
$$= \left[\frac{Q_{\frac{d}{2}}(z)}{\left(\frac{d}{2}+1\right)Q_{\frac{d}{2}-1}(z) - \frac{d^2T}{4e}Q_{\frac{d}{2}}(z)} + \frac{(v-u)^2}{dT}\left(1 - \frac{Q_{\frac{d}{2}-1}(z)}{\left(\frac{d}{2}+1\right)Q_{\frac{d}{2}-1}(z) - \frac{d^2T}{4e}Q_{\frac{d}{2}}(z)}\right)\right]\frac{1}{\rho}\partial_t\rho$$
$$+\left[\frac{(v-u)^2}{2eT}\frac{Q_{\frac{d}{2}-1}(z)}{\left(\frac{d}{2}+1\right)Q_{\frac{d}{2}-1}(z) - \frac{d^2T}{4e}Q_{\frac{d}{2}}(z)} - \frac{d}{2e}\frac{Q_{\frac{d}{2}}(z)}{\left(\frac{d}{2}+1\right)Q_{\frac{d}{2}-1}(z) - \frac{d^2T}{4e}Q_{\frac{d}{2}}(z)}\right]\partial_t e. \tag{7.12}$$

Then if we define $M(z)$ and $N(z)$ as in (3.12), (3.8) follows readily from the above equation.

References

1. Arlotti, L., Lachowicz, M.: Euler and Navier–Stokes limits of the Uehling–Uhlenbeck quantum kinetic equations. J. Math. Phys. **38**, 3571–3588 (1997)
2. Bennoune, M., Lemou, M., Mieussens, L.: Uniformly stable numerical schemes for the Boltzmann equation preserving the compressible Navier–Stokes asymptotics. J. Comput. Phys. **227**, 3781–3803 (2008)
3. Chapman, S., Cowling, T.G.: The Mathematical Theory of Non-Uniform Gases, 3rd edn. Cambridge University Press, Cambridge (1990)
4. Degond, P., Jin, S., Mieussens, L.: A smooth transition model between kinetic and hydrodynamic equations. J. Comput. Phys. **209**(2), 665–694 (2005)
5. Dimarco, G., Pareschi, L.: Fluid solver independent hybrid methods for multiscale kinetic equations. SIAM J. Sci. Comput. **32**(2), 603–634 (2010)
6. Dimarco, G., Pareschi, L.: Exponential Runge–Kutta methods for stiff kinetic equations. SIAM J. Numer. Anal. **49**(5), 2057–2077 (2011)

7. Dimarco, G., Pareschi, L.: High order asymptotic-preserving schemes for the Boltzmann equation. Comptes Rendus Mathematique **350**, 481–486 (2012)
8. Filbet, F., Hu, J., Jin, S.: A numerical scheme for the quantum Boltzmann equation with stiff collision terms. ESAIM Math. Model. Numer. Anal. **46**, 443–463 (2012)
9. Filbet, F., Jin, S.: A class of asymptotic-preserving schemes for kinetic equations and related problems with stiff sources. J. Comput. Phys. **229**, 7625–7648 (2010)
10. Gabetta, E., Pareschi, L., Toscani, G.: Relaxation schemes for nonlinear kinetic equations. SIAM J. Numer. Anal. **34**, 2168–2194 (1997)
11. Garcia, A.L., Wagner, W.: Direct simulation Monte Carlo method for the Uehling–Uhlenbeck–Boltzmann equation. Phys. Rev. E **68**, 056703 (2003)
12. Hairer, E., Nørsett, S.P., Wanner, G.: Solving Ordinary Differential Equations I: Nonstiff Problems (Springer Series in Computational Mathematics). Springer, (2010)
13. Hochbruck, M., Ostermann, A.: Exponential integrators. Acta Numer. **19**, 209–286 (2010)
14. Hu, J., Jin, S.: On kinetic flux vector splitting schemes for quantum Euler equations. Kinet. Relat. Models **4**, 517–530 (2011)
15. Hu, J., Jin, S., Yan, B.: A numerical scheme for the quantum Fokker–Planck–Landau equation efficient in the fluid regime. Commun. Comput. Phys. **12**, 1541–1561 (2012)
16. Hu, J., Ying, L.: A fast spectral algorithm for the quantum Boltzmann collision operator. Commun. Math. Sci. **10**, 989–999 (2012)
17. Jin, S.: Asymptotic preserving (AP) schemes for multiscale kinetic and hyperbolic equations: a review. Riv. Math. Univ. Parma **3**, 177–216 (2012)
18. Jüngel, A.: Transport Equations for Semiconductors. Lecture Notes in Physics, vol. 773. Springer, Berlin (2009)
19. LeVeque, R.J.: Numerical Methods for Conservation Laws. Lectures in Mathematics ETH Zürich. Birkhäuser Verlag (1992)
20. Li, Q., Pareschi, L.: Exponential Runge–Kutta for the inhomogeneous Boltzmann equations with high order of accuracy. J. Comput. Phys. **259**, 402–420 (2014)
21. Li, Q., Yang, X.: Exponential Runge–Kutta methods for the multispecies Boltzmann equation. Commun. Comput. Phys. **15**, 996–1011 (2014)
22. Markowich, P., Pareschi, L.: Fast, conservative and entropic numerical methods for the Bosonic Boltzmann equation. Numer. Math. **99**, 509–532 (2005)
23. Markowich, P., Pareschi, L., Bao, W. Quantum kinetic theory: modelling and numerics for Bose–Einstein condensation. In: Modeling and Computational Methods for Kinetic Equations, Modeling and Simulation in Science, Engineering and Technology, Chapter 10, pp 287–320. Birkhauser, (2004)
24. Markowich, P.A., Ringhofer, C., Schmeiser, C.: Semiconductor Equations. Springer Verlag Wien, New York (1990)
25. Mouhot, C., Pareschi, L.: Fast algorithms for computing the Boltzmann collision operator. Math. Comput. **75**, 1833–1852 (2006)
26. Nordheim, L.W.: On the kinetic method in the new statistics and its application in the electron theory of conductivity. Proc. R. Soc. Lond. Ser. A **119**, 689–698 (1928)
27. Pareschi, L., Caflisch, R.E.: An implicit Monte Carlo method for rarefied gas dynamics i: the space homogeneous case. J. Comput. Phys. **154**, 90–116 (1999)
28. Pareschi, L., Russo, G.: Implicit-explicit Runge–Kutta schemes and applications to hyperbolic systems with relaxation. J. Sci. Comput. **25**(1–2), 129–155 (2005)
29. Pareschi, L., Russo, G.: Efficient asymptotic preserving deterministic methods for the Boltzmann equation. In: Models and Computational Methods for Rarefied Flows. AVT-194 RTO AVT/VKI, Lecture Series held at the von Karman Institute, Rhode St. Genese, Belgium (2011)
30. Pathria, R.K., Beale, P.D.: Statistical Mechanics, 3rd edn. Academic Press, London (2011)
31. Semikoz, D.V., Tkachev, I.I.: Kinetics of Bose condensation. Phys. Rev. Lett. **74**, 3093–3097 (1995)
32. Shu, C.-W.: Essentially Non-Oscillatory and Weighted Essentially Non-Oscillatory Schemes for Hyperbolic Conservation Laws. Technical report, Institute for Computer Applications in Science and Engineering (ICASE) (1997)
33. Spohn, H.: Kinetics of the Bose–Einstein condensation. Phys. D **239**, 627–634 (2010)
34. Tiwari, S., Klar, A.: An adaptive domain decomposition procedure for Boltzmann and Euler equations. J. Comput. Appl. Math. **90**, 223–237 (1998)
35. Uehling, E.A., Uhlenbeck, G.E.: Transport phenomena in Einstein-Bose and Fermi-Dirac gases. I. Phys. Rev. **43**, 552–561 (1933)